# Structure and Reactivity of $[Mo_3\text{-}\mu_3S\text{-}(\mu S_2)_3]^{4+}$ Complexes. Quantum Chemical Calculations, X-ray Structural Characterization, and Raman Spectroscopic Measurements

**María J. Mayor-López and Jacques Weber**

Département de Chimie Physique, Université de Genève, 30 quai Ernest-Ansermet, CH-1211 Genève 4, Switzerland

**Kaspar Hegetschweiler***

Institut für Anorganische Chemie, Universität des Saarlandes, Postfach 15 11 50, D-66041 Saarbrücken, Germany

**Marc D. Meienberger, Felix Joho, Stefano Leoni, and Reinhard Nesper**

Laboratorium für Anorganische Chemie, ETH-Zentrum, CH-8092 Zürich, Switzerland

**Guido J. Reiss and Walter Frank**

Fachbereich Chemie, Universität Kaiserslautern, Erwin-Schrödinger-Strasse, D-67663 Kaiserslautern, Germany

**Boris A. Kolesov, Vladimir P. Fedin, and Vladimir E. Fedorov**

Institute of Inorganic Chemistry, Siberian Branch of the Russian Academy of Sciences, Prospekt Lavrentyeva 3, Novosibirsk, 630090, Russia

*Received September 24, 1997*

A series of compounds containing the $[Mo_3\text{-}\mu_3S\text{-}(\mu S_2)_3\text{-}(dtc)_3]^+$ complex (dtc = diethyldithiocarbamate) with the anions $I^-$ (**1**), $I^-$ and $Br^-$ (**2**), $S^{2-}$ (**3**), $ClO_4^-$ (**4**), $NO_3^-$ (**5**), and $SO_4^{2-}$ (**6**) was prepared and characterized by elemental analysis, NMR, IR, and Raman spectroscopy, and FAB mass spectrometry. The previously reported crystal structure of **1** was reinvestigated. The X-ray analysis revealed the incorporation of $CH_2Cl_2$ in the crystal having the composition $[Mo_3S_7(dtc)_3]I\cdot 0.5CH_2Cl_2$ (**1a**), which was in contradiction to the previous protocol. The corresponding $ClO_4^-$ compound (**4a**) is isotypic. Crystal data: $C_{15.5}H_{31}Cl_2Mo_3N_3O_4S_{13}$, orthorhombic space group *Aba*2, $a = 25.816(5)$ Å, $b = 17.761(4)$ Å, $c = 16.250(3)$ Å, $Z = 8$. For **1a**, **4a**, **6**, and the previously analyzed **2** and **3** the crystal structures revealed characteristic interactions between the anions X and the three axial (out-of-plane) sulfur atoms $S_{ax}$ of the disulfido bridges. The Raman data showed a significant decrease of the $S_{eq}-S_{ax}$ stretch resonance frequency in the order **4**, **5**, **6** > **1** > **3**. This decrease is paralleled with a slight increase of the $S_{eq}-S_{ax}$ bond length and with a significant shortening of the $X\cdots S_{ax}$ distances when compared to the sum of the corresponding van der Waals radii. A comprehensive quantum chemical study, using both density functional theory and semiempirical calculations, revealed that for hard counterions such as $NO_3^-$ and $ClO_4^-$ the $S_{ax}\cdots X$ interactions can be understood in terms of an almost entirely electrostatic interaction, whereas for soft nucleophiles such as $I^-$ and $S^{2-}$ significant covalency is observed. In addition, the general reaction of $[Mo_3S_7]^{4+}$ complexes with a nucleophile was modeled. With regard to the side-on bonding of the $\mu$-$S_2$ groups to Mo, the calculations indicated a significantly higher bond energy for the axial (out-of-plane) sulfur atoms, explaining the much higher lability of the sulfur atoms in the equatorial (in-plane) position. Analogous differences for the ligating atoms of the peripheral ligands, having a cis and trans position with respect to $\mu_3$-S, are less pronounced.

## Introduction

Over the last 15 years, the preparation, reactivity, and molecular structure of complexes containing the $[Mo_3\text{-}\mu_3S\text{-}(\mu S_2)_3]^{4+}$ core have been thoroughly investigated.[1,2] X-ray analyses have revealed a close conformity between the structural parameters of the complex core in a variety of such compounds. The equilateral $Mo_3$ triangle is capped by one apical $\mu_3$-sulfur atom, and in addition each side of the triangle is bridged by a $\mu_2$-disulfido group. The disulfido bridges are oriented perpen-

(1) (a) Müller, A.; Krickemeyer, E. *Inorg. Synth.* **1990**, *27*, 47. (b) Shibahara, T. *Coord. Chem. Rev.* **1993**, *123*, 73.

(2) (a) Virovets, A. V.; Podberezskaya, N. V. *Zh. Strukt. Khim.* **1993**, *34*, 150. (b) Raymond, C. C.; Dorhout, P. K.; Miller, S. M. *Inorg. Chem.* **1994**, *33*, 2703.

* To whom correspondence should be addressed.

S0020-1669(97)01214-7 CCC: $15.00 
Published on Web 05/08/1998

dicular to the $Mo_3$ triangle with the two inequivalent sulfur atoms occupying an equatorial (in-plane) and an axial (out-of-plane) position. The coordination sphere of each Mo atom is completed by additional peripheral ligands which occupy cis and trans positions with respect to the $\mu_3$-sulfur atom. $[Mo_3S(S_2)_3]^{4+}$ complexes are generally highly resistant against acid and oxidizing agents.[3−5] They do, however, react rather readily with a variety of nucleophilic or reducing agents.[6−8] Such reactions can occur either at the Mo atoms or at the disulfido bridges. Nucleophilic attack at a Mo atom results in a simple exchange of a peripheral ligand. Reduction of Mo has, however, not been observed. On the other hand, an attack on the disulfido group leads to sulfur elimination and the formation of a $\mu_2$-S bridge. This can be effectively regarded as a reduction of $S^{-I}$ to $S^{-II}$. A comprehensive electrochemical investigation in aqueous solution provided evidence that the reductive degradation of the disulfido groups also takes place at the surface of a Hg electrode.[7]

A further remarkable property of such $[Mo_3S(S_2)_3]^{4+}$ complexes is their ability to bind an additional anion to the three axial sulfur atoms.[2,6] These interactions are even observed for anionic complexes such as $[Mo_3S_7Br_6]^{2-}$.[9] They have been discussed controversially either as covalent bonding or as an electrostatic interaction.[6,10] In the present investigation, we have used the $[Mo_3S_7(dtc)_3]^+$ complex (dtc = diethyldithiocarbamate) as a model system to elucidate such interactions. A variety of compounds of this complex with different anions have been prepared, and the anion−cation interactions have been characterized by Raman spectroscopy and by crystal structure analyses. The X-ray structure of the $I^-$ adduct, which has been reported previously,[3] was redetermined with the aim of obtaining more precise data for this complex. In addition, we present a theoretical study, using both density functional theory (DFT) and semiempirical calculations, for the following molecular systems: the $[Mo_3S_7]^{4+}$ core and its charged and neutral derivatives $[Mo_3S_7(S_2)_3]^{2-}$, $[Mo_3S_7Cl_6]^{2-}$, $[Mo_3S_7L_3]ClO_4$, $[Mo_3S_7L_3]Cl$, and the dimeric $[Mo_3S_7L_3]_2S$ (where L = $H-CS_2^-$, representing a simplified model of $dtc^-$). The purpose of this theoretical analysis is to attempt to rationalize the general reactivity of $Mo_3S_7$ complexes with nucleophiles.

## Experimental Section

**Analyses and Spectroscopy.** $[Mo_3S_7(dtc)_3]Br_{0.113}I_{0.887}$ (**2**) was analyzed by the Laboratorium für Elemente- und Mikroanalytik, Ciba-Geigy AG, Basel, Switzerland. The C,H,N analyses of all other compounds were performed by D. Manser, Laboratorium für Organische Chemie, ETH Zürich, Switzerland, and Mo was determined spectrophotometrically as bis(tironato)molybdenum(VI) (390 nm) after digestion of the sample in aqua regia. $^1H$ and $^{13}C$ NMR spectra were recorded on a Bruker AMX-500 spectrometer. $FAB^+$ MS measurements were performed on a VG ZAB VSEQ instrument. The samples were dissolved in $CH_2Cl_2$, and the resulting solutions were then mixed with a 3-nitrobenzyl alcohol matrix prior to introduction into the spectrometer. IR spectra were recorded on a IFS-113 FT-IR spectrometer. The solid samples were dispersed in poly(chlorotrifluoroethylene) oil (3800−2100 $cm^{-1}$) or in Nujol (2100−400 $cm^{-1}$). Raman spectra of the solid samples were measured at room temperature in backscattering geometry by using the 514.5 nm Ar laser line (Coherent INNOVA 90-4) as the excitation source. The probe laser beam was focused to a spot diameter of about 1 $\mu$m, and a low incident power at the sample microcrystal surface of 0.5 mW was used. The Raman signal was detected with the multichannel spectrometer DILOR-XY. Calibration of the spectrometer was performed by the spectral position of the laser line. The spectra were recorded with a resolution of 0.5 $cm^{-1}$.

**$[Mo_3S_7(dtc)_3]I$ (1)**. The two compounds named modification 1 and modification 2 in our previous report[3] were prepared as described. Modification 1 was obtained by the oxidation of $(NH_4)_2[Mo_3S_{13}]$ with $dtc_2$ (= $Et_2N-CS-S-S-CS-NEt_2$). Single crystals of the composition $[Mo_3S_7(dtc)_3]I\cdot 0.5CH_2Cl_2$ (**1a**) were grown from *n*-hexane/$CH_2Cl_2$. Raman ($cm^{-1}$): 146.6 m, 225.8 w, 252.9 m, 278.4 s, 320.6 w, 361.1 m, 373.6 w, 392.9 m, 401.8 w, 454.3 w, 519.7 s, 528.4 s.

Modification 2, which was prepared by the reaction of $(NEt_4)_2[Mo_3S_7Br_6]$ with Na(dtc), proved to be a mixture of a $Br^-$ and an $I^-$ adduct. Anal. Calcd for $[C_{15}H_{30}Mo_3N_3S_{13}]Br_{0.113}I_{0.887}$ (**2**): C, 16.70; H, 2.80; Br, 0.84; I, 10.44; N, 3.90; Mo, 26.68; S, 38.64. Found: C, 16.80; H, 2.83; Br, 0.84; I, 10.45; N, 3.98; Mo, 26.0; S, 38.51.

**$[Mo_3S_7(dtc)_3]_2S$ (3).** A solution of $[Mo_3S_7(dtc)_3]dtc$ (11 mg, 10 $\mu$mol)[10] in 2 mL of $CH_2Cl_2$ was layered with 2 mL of aqueous KOH solution (1 M). The brown crystals which formed within 2 weeks were collected and dried in air. Yield: 25%. Anal. Calcd for $C_{30}H_{60}Mo_6N_6S_{27}$: C, 18.51; H, 3.11; N, 4.32; Mo 29.58. Found: C, 18.83; H, 3.10; N, 4.28; Mo, 29.82. IR ($cm^{-1}$): 2980 m, 2940 w, 2860 w, 1500 s, 1450 m, 1430 s, 1370 m, 1350 m, 1300 w, 1270 s, 1200 m, 1150 m, 1060 m, 1000 m, 960 w, 910 m, 840 m, 770 m, 700 w, 660 w, 600 w, 560 w, 550 w. Raman ($cm^{-1}$): 145.8 s, 231.8 m, 255.2 w, 279.4 s, 312.9 m, 348.8 m, 371.4 m, 393.9 s, 449.6 w, 504.1 w, 611.2 w, 778.7 w.

**$[Mo_3S_7(dtc)_3]ClO_4$ (4)** was prepared from $[Mo_3S_7(dtc)_3]Br$ (100 mg, 96.4 $\mu$mol),[3] dissolved in 30 mL of DMF, by anion exchange on Dowex 1 X4 (50−100 mesh, from Fluka). The resin ($Cl^-$ form) was placed in a column (1.5 × 25 cm), and $Cl^-$ was replaced by $ClO_4^-$ by rinsing of the column with a saturated aqueous solution of $NaClO_4$ until the eluent was free of $Cl^-$ (checked with $AgNO_3$). The column was then rinsed with an excess of DMF, and the $[Mo_3S_7(dtc)_3]Br$ solution was passed slowly through the column. The orange fraction was collected and evaporated to dryness under reduced pressure at a bath temperature of <40 °C. **CAUTION! The resulting perchlorate adduct 4 is potentially explosive. It should only be prepared in small quantities and must be handled with care.** The product was recrystallized from a 1:1 mixture of *n*-hexane and $CH_2Cl_2$ and dried in vacuo (0.01 mbar, 25 °C). Anal. Calcd for $C_{15}H_{30}ClMo_3N_3O_4S_{13}$: C, 17.05; H, 2.86; N, 3.98; Mo, 27.24. Found: C, 17.21; H, 2.79; N, 4.13; Mo, 27.04. The NMR data and the $FAB^+$ mass spectrum of this product were identical with those of **1**.[3] IR ($cm^{-1}$): 2970 m, 2930 m, 2850 w, 1640 m, 1510 s, 1440 s, 1380 m, 1350 m, 1280 s, 1200 m, 1100 s, 1000 m, 910 w, 850 m, 780 w, 620 m, 560 m, 400 w, 370 w. Raman ($cm^{-1}$): 100.4 s, 131.5 s, 147.5 m, 224.3 s, 255.2 m, 280.3 s, 288.6 s, 305.4 m, 366.4 s, 376.4 m, 394.7 w, 456.2 w 568.5 s. Single crystals of the composition $[Mo_3S_7(dtc)_3]ClO_4\cdot 0.5CH_2Cl_2$ (**4a**) were grown from *n*-hexane/$CH_2Cl_2$. In their mother liquor, the crystals were stable indefinitely, but they rapidly disintegrated upon exposure to air.

**$[Mo_3S_7(dtc)_3]NO_3\cdot CH_2Cl_2$ (5)** was prepared by the same procedure as reported for **4** using Dowex 1 X4 resin in the $NO_3^-$ form. Anal. Calcd for $C_{16}H_{32}Cl_2Mo_3N_4O_3S_{13}$: C, 17.41; H, 2.92; N, 5.07; Mo, 26.07. Found: C, 17.37; H, 3.00; N, 5.11; Mo, 25.84. The incorporation of

(3) Zimmermann, H.; Hegetschweiler, K.; Keller, T.; Gramlich, V.; Schmalle, H. W.; Petter, W.; Schneider, W. *Inorg. Chem.* **1991**, *30*, 4336.
(4) Hegetschweiler, K.; Keller, T.; Zimmermann, H.; Schneider, W.; Schmalle, H.; Dubler, E. *Inorg. Chim. Acta* **1990**, *169*, 235.
(5) Fedin, V. P.; Sokolov, M. N.; Mironov, Yu. V.; Kolesov, B. A.; Tkachev, S. V.; Fedorov, V. Ye. *Inorg. Chim. Acta* **1990**, *167*, 39.
(6) Meienberger, M. D.; Hegetschweiler, K.; Rüegger, H.; Gramlich, V. *Inorg. Chim. Acta* **1993**, *213*, 157.
(7) Hegetschweiler, K.; Keller, T.; Bäumle, M.; Rihs, G.; Schneider, W. *Inorg. Chem.* **1991**, *30*, 4342.
(8) (a) Müller, A.; Reinsch, U. *Angew. Chem.* **1980**, *92*, 69. (b) Keck, H.; Kuchen, W.; Mathow, J.; Wunderlich, H. *Angew. Chem.* **1982**, *94*, 927. (c) Halbert, T. R.; McGauley, K.; Pan, W.-H.; Czernuszewicz, R. S.; Stiefel, E. I. *J. Am. Chem. Soc.* **1984**, *106*, 1849. (d) Cotton, F. A.; Kibala, P. A.; Matusz, M.; McCaleb, C. S.; Sandor, R. B. W. *Inorg. Chem.* **1989**, *28*, 2623.
(9) Fedorov, V. Ye.; Geras'ko, O. A.; Mironov, Yu. V.; Hegetschweiler, K.; Stoop, R.; Gallus, J.; Gramlich, V. *Russ. J. Struct. Chem.* **1995**, *36*, 1046.
(10) Fedin, V. P.; Sokolov, M. N.; Geras'ko, O. A.; Virovets, A. V.; Podberezskaya, N. V.; Fedorov, V. Ye. *Inorg. Chim. Acta* **1992**, *192*, 153.

**Table 1.** Crystallographic Data for $[Mo_3S_7(dtc)_3]I\cdot 0.5CH_2Cl_2$ (**1a**) and $[Mo_3S_7(dtc)_3]ClO_4\cdot 0.5CH_2Cl_2$ (**4a**)

| compound | **1a** | **4a** |
|---|---|---|
| empirical formula | $C_{15.5}H_{31}ClIMo_3N_3S_{13}$ | $C_{15.5}H_{31}Cl_2Mo_3N_3O_4S_{13}$ |
| fw | 1126.4 | 1099.0 |
| space group | *Aba*2 (No. 41) | *Aba*2 (No. 41) |
| *a*, Å | 24.782(2) | 25.816(5) |
| *b*, Å | 17.849(3) | 17.761(4) |
| *c*, Å | 16.429(3) | 16.250(3) |
| *V*, Å$^3$ | 7267(2) | 7451(3) |
| *Z* | 8 | 8 |
| *T*, °C | 20(2) | −93(2) |
| $\lambda$ (Mo Kα), Å | 0.710 73 | 0.710 73 |
| $\rho_{calcd}$, g cm$^{-3}$ | 2.06 | 1.96 |
| $\mu$(Mo Kα), cm$^{-1}$ | 27.06 | 18.90 |
| $R_1$ [$I > 2\sigma(I)$][a] | 0.0350 | 0.0393 |
| w$R_2$ (all data)[b] | 0.0540 | 0.1135 |

[a] $R = \sum(||F_o| - |F_c||)/\sum|F_o|$. [b] $wR_2 = [\sum w(F_o^2 - F_c^2)^2/\sum wF_o^4]^{1/2}$.

1 equiv of $CH_2Cl_2$ was confirmed by $^1$H and $^{13}$C NMR spectroscopy. Otherwise the NMR and FAB$^+$ data were identical with those of **1**.[3] In contrast to **1** and **4**, drying in vacuo did not result in a loss of the incorporated $CH_2Cl_2$. IR (cm$^{-1}$): 2970 s, 2930 s, 2870 m, 1640 m, 1510 s, 1440 s, 1380 s, 1360 s, 1280 s, 1200 s, 1150 s, 1070 s, 1000 m, 910 m, 850 m, 830 m, 780 m, 700 w, 600 m, 560 m, 530 m, 490 w, 480 w, 460 w, 440 w, 430 w, 400 w, 370 m, 330 w, 320 w. Raman (cm$^{-1}$): 154.2 m, 165.9 s, 224.3 w, 281.1 s, 307.0 w, 367.2s, 395.6 w, 419.7 w, 452.9 m, 563.6 s, 741.7 w.

**$[Mo_3S_7(dtc)_3]_4(SO_4)_2\cdot 3THF$ (6).** $[Mo_3S_7(dtc)_3]NO_3\cdot CH_2Cl_2$ (**5**, 110 mg, 100 $\mu$mol) was dissolved in 30 mL of DMF and the mixture heated to 90 °C for 1 h. The solution was then evaporated to dryness under reduced pressure, and the resulting solid was recrystallized from $CH_2Cl_2$/THF and dried in vacuo. Yield: 50%. Anal. Calcd for $C_{72}H_{144}Mo_{12}N_{12}O_{11}S_{54}$: C, 20.41; H, 3.43; N, 3.97. Found: C, 20.25; H, 3.64; N, 3.84. The incorporation of THF into the solid **6** was confirmed by $^1$H and $^{13}$C NMR spectroscopy. Otherwise the NMR data and the FAB$^+$ MS characteristics were identical with those of **1**.[3] Raman (cm$^{-1}$): 142.3 m, 230.1 w, 254.0 m, 278.9 s, 293.2 w, 307.4 w, 364.2 s, 395.0 s, 420.5 w, 461.0 w, 549.9 s, 557.6 m. Single crystals were grown by dissolving the solid in $CH_2Cl_2$ and layering the solution with an equal volume of THF.

**Crystal Structure Determination.** Crystal data for **1a** and **4a** are presented in Table 1. Atomic coordinates and the crystallographic data for **6** are provided as Supporting Information. Selected bond distances and bond angles are summarized in Table 2. Additional information on data collection, structure solution, and refinement is summarized below.

X-ray data for $[Mo_3S_7(dtc)_3]I\cdot 0.5CH_2Cl_2$ (**1a**) were collected at 293(2) K on a red crystal, having approximate dimensions of 0.36 × 0.24 × 0.11 mm using a Siemens P4 four circle diffractometer and graphite-monochromated Mo Kα radiation. The stability of the crystal was checked by measuring three standard reflections after every 100 reflections. No decrease of intensity was noted. A numerical absorption correction was applied ($T_{min} = 0.451$, $T_{max} = 0.618$), and the data were corrected for Lorentz and polarization effects. The structure was solved by Patterson methods (SHELXS-86);[11] 6774 unique data were used for the refinement of 331 parameters (SHELXL93,[12] full-matrix least-squares calculations on $F^2$, anisotropic displacement parameters for all non-hydrogen atoms). The positions of the H atoms were calculated and included in the refinement using a riding model and fixed isotropic displacement parameters. The absolute structure parameter[13] was found to be 0.01(1).

An orange crystal of $[Mo_3S_7(dtc)_3]ClO_4\cdot 0.5CH_2Cl_2$ (**4a**) was sealed in a glass capillary together with its mother liquor; 10 540 intensity data were collected at 180(2) K using a STOE IPDS image plate system and graphite-monochromated Mo Kα radiation. An absorption correction was not performed. The structure was solved by direct methods (SHELXS-86);[11] 3140 unique data were used for the refinement of 379 parameters (SHELXL93,[12] full-matrix least-squares calculations on $F^2$, anisotropic displacement parameters for all non-hydrogen atoms). The positions of the H atoms were calculated and included in the refinement using a riding model and fixed isotropic displacement parameters. The absolute structure parameter[13] was found to be −0.01(7).

**Theoretical Calculations.** DFT calculations have been performed using the Amsterdam Density Functional package ADF developed by Baerends et al.[14−16] The numerical integration procedure employed for the calculations was developed by te Velde et al.[16,17] An uncontracted double-$\zeta$ STO basis set[18] has been used for 4s, 4p, and 4d orbitals of molybdenum atoms, for *n*s and *n*p orbitals of sulfur, oxygen, chlorine, and carbon atoms, and for 1s orbitals of H atoms. This basis set has been augmented by a p polarization function in the case of Mo and H, whereas for S, O, Cl, and C atoms an extra d polarization function has been added. The inner cores of molybdenum (1s2s2p3s3p3d), sulfur (1s2s2p), carbon (1s), oxygen (1s), and chlorine (1s2s2p) have been treated with the frozen-core approximation.[15] A set of auxiliary s, p, d, f, and g STO functions,[19] centered on all nuclei, has been used to fit the molecular density and to represent the Coulomb and exchange potentials accurately in each SCF cycle.

The calculations have been performed at different levels of theory. Geometry optimizations and linear transit calculations have been mostly achieved at the LDA (local density approximation)[20] level where the VWN (Vosko−Wilk−Nusair)[21] approximation has been used. In some cases Stoll's[22] correction to the VWN formulas has been added. For energy calculations a higher level of theory may be required, and in some test calculations performed for the $[Mo_3S(S_2)_3]^{4+}$ cluster core, the local approximation has been augmented by gradient-based nonlocal corrections to the exchange and correlation potentials due to Becke[23] and Perdew[24] (BP), respectively. These corrections have been included in the SCF procedure[25] (NL-SCF calculation). As ADF molecular energies represent actual bonding energies between fragments,[26] the same fragments were always used as building blocks for the various structures of the systems in order to have meaningful results.

**Semiempirical Methods.** Two different semiempirical methods have been applied, using the ADF-optimized geometries: standard extended Hückel (EH)[27] calculations to analyze the electronic structure of these systems and the EH-based reactivity index (EHPROP) to describe their reactivity.[28,29] The latter model is based on the calculation of the intermolecular interaction energy $E_{int}$ between a substrate Sbst and a model nucleophile reactant R. The reactive properties of Sbst in the presence of R are described by using the calculated Sbst−R intermolecular interaction energy calculated as a local reactivity index,

(11) Sheldrick, G. M. SHELXS-86. *Acta Crystallogr., Sect. A* **1990**, *46*, 467.
(12) Sheldrick, G. M. *SHELXL-93. A program for the refinement of crystal structures*; University of Göttingen: Göttingen, 1993.
(13) Flack, H. D. *Acta Crystallogr., Sect. A* **1983**, *39*, 876.
(14) ADF 2.0.1, Department of Theoretical Chemistry, Vrije Universiteit: Amsterdam, The Netherlands, 1995.
(15) Baerends, E. J.; Ellis, D. E.; Ros, P. *Chem. Phys.* **1973**, *2*, 41.
(16) te Velde, G.; Baerends, E. J. *J. Comput. Phys.* **1992**, *99*, 84.
(17) Boerritger, P. M.; te Velde, G.; Baerends, E. J. *Int. J. Quantum Chem.* **1988**, *33*, 87.
(18) Vernooijs, P.; Snijders, J. G.; Baerends, E. J. Slater Type Basis Functions for the Whole Periodic System. Internal Report; Vrije Universiteit: Amsterdam, The Netherlands, 1981.
(19) Krijn, K.; Baerends, E. J. Fit Functions in the HFS Method, Internal Report; Vrije Universiteit: Amsterdam, The Netherlands, 1984.
(20) Gunnarsson, O.; Lundquist, I. *Phys. Rev.* **1974**, *B10*, 1319.
(21) Vosko, S. H.; Wilk, L.; Nusair, M. *Can. J. Phys.* **1980**, *58*, 1200.
(22) Stoll, H.; Pavlidou, C. M. E.; Preuss, H. *Theor. Chim. Acta* **1978**, *49*, 143.
(23) Becke, A. D. *Phys. Rev.* **1988**, *A38*, 3098.
(24) Perdew, J. P. *Phys. Rev.* **1986**, *B33*, 8822.
(25) Fan, L.; Ziegler, T. *J. Chem. Phys.* **1991**, *94*, 6057.
(26) Ziegler, T.; Rauk, A. *Theor. Chim. Acta* **1977**, *49*, 143.
(27) Hoffmann, R. *J. Chem. Phys.* **1963**, *39*, 1397.
(28) Daul, C.; Goursot, A.; Morgantini, P. Y.; Weber, J. *Int. J. Quantum Chem.* **1990**, *38*, 623.
(29) Weber, J.; Stussi, D.; Flükiger, P.; Morgantini, P. Y. *Comments Inorg. Chem.* **1992**, *14*, 27.

**Table 2.** Selected Summarized Bond Lengths (Å) and Bond Angles (deg) of $[Mo_3S_7(dtc)_3]I\cdot 0.5CH_2Cl_2$ (**1a**) and $[Mo_3S_7(dtc)_3]ClO_4\cdot 0.5CH_2Cl_2$ (**4a**)

| | **1a** | | **4a** | |
|---|---|---|---|---|
| | mean | range | mean | range |
| Mo−Mo′ | 2.718 | 2.7095(8)−2.7255(9) | 2.711 | 2.700(1)−2.717(1) |
| Mo-$\mu_3$S | 2.373 | 2.372(2)−2.375(2) | 2.377 | 2.374(3)−2.381(2) |
| Mo−$S_{eq}$ | 2.488 | 2.476(2)−2.501(2) | 2.484 | 2.471(2)−2.496(2) |
| Mo−$S_{ax}$ | 2.415 | 2.410(2)−2.422(2) | 2.407 | 2.403(2)−2.410(3) |
| Mo−$S_{cis}$ | 2.468 | 2.462(2)−2.479(2) | 2.461 | 2.457(3)−2.465(2) |
| Mo−$S_{trans}$ | 2.524 | 2.521(2)−2.529(2) | 2.512 | 2.503(2)−2.527(3) |
| S−S | 2.055 | 2.050(3)−2.059(2) | 2.027 | 2.019(5)−2.035(4) |
| C−$S_{cis}$ | 1.719 | 1.709(8)−1.731(7) | 1.711 | 1.704(9)−1.72(2) |
| C−$S_{trans}$ | 1.727 | 1.725(8)−1.729(7) | 1.718 | 1.71(1)−1.72(1) |
| N−C($sp^2$) | 1.313 | 1.308(8)−1.319(9) | 1.332 | 1.33(1)−1.34(1) |
| N−C($sp^3$) | 1.491 | 1.450(9)−1.526(10) | 1.465 | 1.44(2)−1.50(2) |
| C−C | 1.49 | 1.43(1)−1.52(1) | 1.49 | 1.46(2)−1.51(2) |
| C−Cl | 1.69(1) | | 1.75 | 1.64(4)−1.85(5) |
| Cl−O | | | 1.426 | 1.41(1)−1.448(7) |
| Mo′−Mo−Mo″ | 60.00 | 59.67(2)−60.26(2) | 60.00 | 59.61(3)−60.21(2) |
| $S_{ax}$−Mo−$S'_{ax}$ | 85.29 | 84.87(6)−85.62(6) | 85.78 | 85.6(1)−86.07(9) |
| $S_{ax}$−Mo−$S_{eq}$ | 49.55 | 49.31(6)−49.77(6) | 48.95 | 48.83(8)−49.16(9) |
| $S_{ax}$−Mo−$S'_{eq}$ | 134.55 | 134.10(7)−134.84(6) | 134.47 | 134.29(9)−134.74(8) |
| $S_{ax}$−Mo−$S_{cis}$ | 133.29 | 131.14(7)−135.96(6) | 132.86 | 130.61(9)−135.43(8) |
| $S_{ax}$−Mo−$S_{trans}$ | 88.85 | 88.44(6)−89.21(7) | 88.31 | 87.24(7)−89.28(9) |
| $S_{eq}$−Mo−$S'_{eq}$ | 170.69 | 170.03(7)−171.15(7) | 171.32 | 170.4(1)−171.94(8) |
| $S_{eq}$−Mo−$S_{cis}$ | 89.60 | 87.09(7)−92.21(7) | 89.89 | 87.29(9)−92.44(9) |
| $S_{eq}$−Mo−$S_{trans}$ | 94.23 | 93.84(7)−94.57(7) | 94.05 | 92.36(7)−95.34(8) |
| $S_{cis}$−Mo−$S_{trans}$ | 70.37 | 70.23(6)−70.59(6) | 70.48 | 70.4(1)−70.59(9) |
| $\mu_3$S−Mo−$S_{ax}$ | 110.20 | 109.92(6)−110.70(6) | 110.28 | 109.94(9)−110.76(7) |
| $\mu_3$S−Mo−$S_{eq}$ | 85.35 | 84.87(7)−85.78(6) | 85.68 | 85.16(9)−86.52(9) |
| $\mu_3$S−Mo−$S_{cis}$ | 83.24 | 82.90(7)−83.84(6) | 83.59 | 83.32(8)−83.9(1) |
| $\mu_3$S−Mo−$S_{trans}$ | 153.58 | 153.22(7)−154.06(6) | 154.07 | 153.7(1)−154.31(9) |
| Mo−$S_{ax}$−Mo′ | 68.52 | 68.18(5)−68.85(5) | 68.56 | 68.36(6)−68.70(7) |
| Mo−$S_{ax}$−$S_{eq}$ | 67.08 | 66.52(7)−67.66(7) | 67.51 | 67.2(1)−67.91(9) |
| Mo−$S_{eq}$−Mo′ | 66.24 | 66.20(5)−66.30(5) | 66.16 | 66.11(6)−66.19(6) |
| Mo−$S_{eq}$−$S_{ax}$ | 63.37 | 63.03(7)−63.77(7) | 63.54 | 63.23(9)−63.8(1) |
| Mo-$\mu_3$S−Mo | 69.88 | 69.63(5)−70.06(5) | 69.54 | 69.18(7)−69.77(8) |
| O−Cl−O | | | 109.47 | 108.9(6)−110.2(5) |

which can be also visualized[30] to rationalize nucleophilic substitution mechanisms. The expression of the intermolecular interaction energy $E_{int}$ is $E_{int}(\mathbf{r}) = E_{es}(\mathbf{r}) + E_{ct}(\mathbf{r}) + E_{ex}(\mathbf{r})$ where **r** specifies the position of the incoming reactant, $E_{es}$, $E_{ct}$, and $E_{ex}$ being the electrostatic, charge-transfer, and exchange-repulsion energy components, respectively, calculated in the EH framework. Details of such calculations have been reported previously.[28,29]

## Results

**Preparation and Structural Characterization.** A series of adducts $[Mo_3S_7(dtc)_3]X$ (where X represents a mononegative anion such as $ClO_4^-$ or $NO_3^-$) could be readily obtained by passing a DMF solution of the conveniently prepared starting material $[Mo_3S_7(dtc)_3]Br$ through a column of anion-exchange resin.[3] The preparation and structure of analogous adducts with $Cl^-$ and $TCNQ^-$ (=7,7,8,8-tetracyanoquinodimethane) have been reported elsewhere.[10,31] Adducts with the doubly charged anions $S^{2-}$ and $SO_4^{2-}$ were prepared by hydrolysis or oxidation of the dtc ligand, respectively.

The X-ray structure of $[Mo_3S_7(dtc)_3]I$ has been published by three independent research groups. Fedin et al. obtained the benzene solvate $[Mo_3S_7(dtc)_3]I\cdot 1.5C_6H_6$, which crystallized in the rhombohedral space group $R\bar{3}c$.[32] Lu et al. isolated $[Mo_3S_7(dtc)_3]I$ from DMF and observed no incorporation of any solvent.[33] They found that the complex crystallizes in the monoclinic space group $P2_1/n$. In our own previous protocol,[3] we claimed that this compound, isolated from $CH_2Cl_2$/EtOH (modification 1), crystallized in the orthorhombic, face-centered space group *Aba*2. However, a second modification, isolated from a mixture of DMF, EtOH, and $Et_2O$ (modification 2 in our previous report), crystallized in the orthorhombic, body-centered space group *Iba*2. It is evident that a different packing and, thus, a different space group are observed for Fedin's benzene solvate on the one hand and the solvent-free complex on the other. However, it is rather puzzling that three different space groups were reported for the latter. Since $[Mo_3S_7(dtc)_3]I$ is a key complex in the present investigation, we decided to reinvestigate its composition and crystal structure. The compound, named modification 2, was obtained from $[Mo_3S_7Br_6]^{2-}$ by ligand exchange (reaction with Na-dtc) followed by precipitation of the iodide adduct $[Mo_3S_7(dtc)_3]I$ by addition of excess NaI. Consequently the incorporation of $I^-$ and $Br^-$ in the solid phase should have been considered. Careful analysis did indeed reveal that the material used for X-ray analysis still contained traces of $Br^-$ and must be formulated as $[Mo_3S_7(dtc)_3]Br_{0.113}I_{0.887}$ (**2**). According to the crystal structure analysis,[3] $Br^-$ and $I^-$ occupy the anion position at random. Modification 1 analyzed as $[Mo_3S_7(dtc)_3]I$ (**1**) after drying in vacuo. However, careful reinvestigation of the crystal structure revealed that after recrystallization from $CH_2Cl_2$/*n*-hexane (**1a**), 0.5 equiv of $CH_2$-

(30) Flükiger, P. Development of the Molecular Graphics Package MOLEKEL and its Application to Selected Problems in Organic and Organometallic Chemistry. Ph.D. Thesis No. 2561, University of Geneva, Switzerland, 1992.
(31) Fedin, V. P.; Sokolov, M. N.; Virovets, A. V.; Podberezskaya, N. V.; Fedorov, V. Ye. *Inorg. Chim. Acta* **1992**, *194*, 195.
(32) Fedin, V. P.; Müller, A.; Bögge, H.; Armatage, A.; Sokolov, M. N.; Yarovoi, S. S.; Fedorov, V. E. *Russ. J. Inorg. Chem.* **1993**, *38*, 1563.
(33) Lu, C.-Z.; Tong, W.; Zhuang, H.-H.; Wu, D.-M. *Jiegou Huaxue* **1993**, *12*, 124.

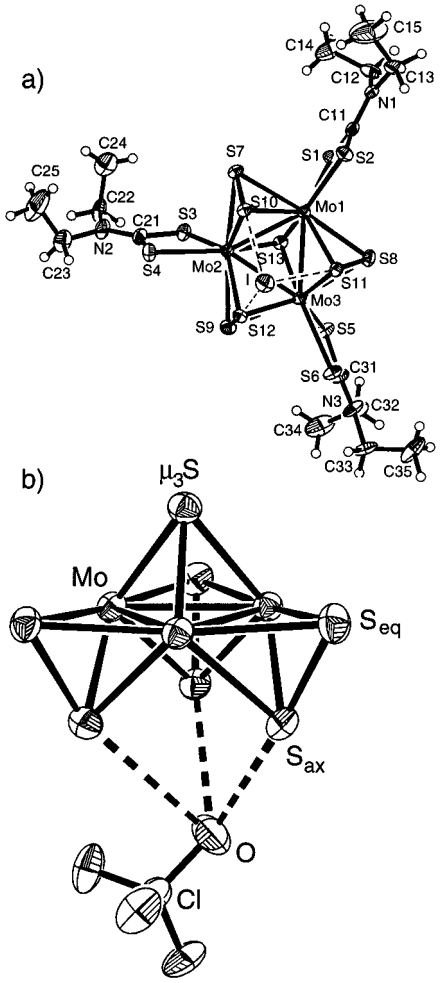


**Figure 1.** Crystal structure of $[Mo_3S_7(dtc)_3]^+$. (a) View of the $I^-$ adduct **1a** with numbering scheme. (b) Illustration of the anion−cation interaction in the $ClO_4^-$ adduct **4a** (the peripheral dtc ligands are omitted for clarity). The vibrational ellipsoids correspond to the 50% probability level.

$Cl_2$ was incorporated into the structure. It is noteworthy that the lattice parameters, space group, and habit of **1a** were in close agreement with those reported previously for "modification 1", and that $CH_2Cl_2$ has been used for crystal growth in both cases. It is of course possible that in the previous sample $CH_2Cl_2$ has not been incorporated (the absence of $CH_2Cl_2$ would then explain the disorder of the ethyl groups observed only in the previous investigation). However, we cannot exclude the possibility that due to the lower quality of the previous structure analysis[34] the presence of an incorporated solvent molecule has been overlooked.

The crystal structures of the $I^-$ adduct **1a** and the $ClO_4^-$ adduct **4a** are isomorphous, and the $ClO_4^-$ counterion is found on the same position as the $I^-$ in **1a** (Figure 1). However, the mean $ClO_4^-\cdots S_{ax}$ distance of 3.013 Å is only slightly shorter than the sum of the van der Waals radii of S and O. Moreover, in the structure of adduct **1a**, the incorporated $CH_2Cl_2$ solvent molecule is precisely placed on the 2-fold axis, whereas in **4a**, the solvent molecule is found to be disordered over two sites. This is in agreement with the observed difference in crystal stability. Crystals of **1a** were stable in air for an unlimited period of time, whereas the crystals of **4a** disintegrate rapidly upon exposure to air and they must be stored in their mother liquor.

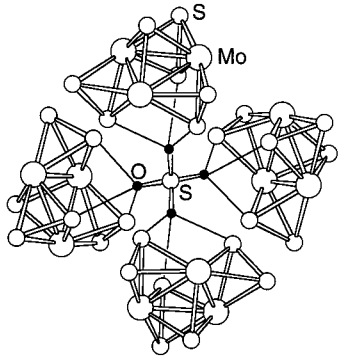


**Figure 2.** Ball and stick representation of the tetrameric $[Mo_3S_7(dtc)_3]_4$-$SO_4^{2+}$ entity, found in the crystal structure of **6**. Mo, S, and O atoms are shown as spheres with a decreasing radius in this order. The peripheral dtc ligands are omitted for clarity.

Crystals of the $SO_4^{2-}$ adduct **6** grown from $CH_2Cl_2$/THF proved to be of low quality. An X-ray analysis revealed the positions of all non-hydrogen atoms of the $[Mo_3S_7(dtc)_3]_4$-$(SO_4)^{2+}$ entity, but a second sulfate counterion and several solvent molecules proved to be severely disordered.[35] Consequently, any discussion of structural parameters such as bond lengths and angles is inappropriate. However, the structure does allow an unambiguous assignment of the connectivity of this cluster. In contrast to the $ClO_4^-$ adduct **4a**, where the structure is made up of discrete 1:1 ion pairs, **6** consists of a tetrameric arrangement, where the central $SO_4^{2-}$ entity interacts with four different $[Mo_3S_7(dtc)_3]^+$ molecules. As shown in Figure 2, each of the four oxygen atoms of $SO_4^{2-}$ is directed toward three axial sulfur atoms of a $Mo_3S_7$ cluster.

The anion−cation interactions of the complexes **1**−**6** were further investigated by Raman spectroscopy. The resonance frequencies were assigned to corresponding valence force constants on the basis of a previously reported normal vibrational analysis.[5,10,36] Frequencies in the range 500−570 $cm^{-1}$ are of particular relevance, because they are predominantly related to the valence (stretching) vibrations of the $\mu_2$-($S_{eq}$−$S_{ax}$) bridges. The results are summarized in Table 3, and the correlations with the $S_{eq}$−$S_{ax}$ and $S_{ax}\cdots X$ distances are illustrated in Figure 3. These findings clearly indicate that the force constants of the $S_{eq}$−$S_{ax}$ bonds are rather sensitive to the nature of the anion. For hard anions such as $ClO_4^-$ or $NO_3^-$, the frequencies are at the high end of this range (560−570 $cm^{-1}$), whereas for the soft $I^-$ and $S^{2-}$, lower frequencies (528 and 504 $cm^{-1}$) were noted. The decrease of the $S_{eq}$−$S_{ax}$ force constants is clearly correlated with an increasing elongation of the $S_{ax}$−$S_{eq}$ bond

(34) In the previous analysis, a rather small crystal (0.1 × 0.1 × 0.07 mm) was used and an absorption correction was not performed. The refinement using 2067 reflections and isotropic displacement parameters for the C and N atoms gave $R = 0.063$ and $R_w = 0.090$.

(35) $[Mo_3S_7(dtc)_3]_4(SO_4)_2\cdot 3THF$ (**6**) crystallizes in the hexagonal space group $P6_222$, $a = 23.888(3)$ Å, $c = 31.844(6)$ Å, $C_{18}H_{36}Mo_3N_3O_{2.75}S_{13.5}$, $Z = 12$. The second $SO_4^{2-}$ counterion and the three THF molecules as required from elemental analyses and NMR spectroscopic measurements were severely disordered and could not be assigned to a chemically sensitive model. All non-hydrogen positions of the tetrameric $[Mo_3S_7(dtc)_3]_4(SO_4)^{2+}$ entity were refined (on $F^2$) using anisotropic displacement parameters. Hydrogen atoms were placed at calculated positions. $R_1 = 5.76\%$ for 3938 observed reflections with $I > 2\sigma(I)$ and $wR_2 = [\sum w(F_o^2 - F_c^2)^2/\sum wF_o^4]^{1/2} = 20.3\%$ for all 4040 unique data and 375 refined parameters (STOE IPDS image plate system, graphite-monochromated Mo Kα radiation, 20 °C). Further crystallographic data, atomic coordinates, and a list of bond distances and angles are provided as supplementary data (see Supporting Information).

(36) Fedin, V. P.; Kolesov, B. A.; Mironov, Yu. V.; Fedorov, V. Ye. *Polyhedron* **1989**, *8*, 2419.

**Table 3.** Mean Interatomic Distances $d(S_{eq}-S_{ax})$ and $d(S_{ax}\cdots X)$, Covalency Index $f_{cov}$ for the $S_{ax}\cdots X$ Interaction,[a] and Raman Frequency $\nu$ of the $S_{eq}-S_{ax}$ Stretching Mode of a Variety of $[Mo_3S_7(dtc)_3]X$ Adducts (dtc = diethyldithiocarbamate)

| | $d(S_{eq}-S_{ax})$, Å | $d(S_{ax}-X)$, Å | $f_{cov}$[a] | $\nu(S_{eq}-S_{ax})$, $cm^{-1}$ |
|---|---|---|---|---|
| $[Mo_3S_7(dtc)_3]ClO_4$[b] | 2.027 | 3.013 | 0.21 | 569 |
| $[Mo_3S_7(dtc)_3]Cl$[c] | 2.041 | 2.996 | 0.40 | 543 |
| $[Mo_3S_7(dtc)_3]I$[b] | 2.055 | 3.269 | 0.43 | 528 |
| $[Mo_3S_7(dtc)_3]_2S$[d] | 2.113 | 2.713 | 0.60 | 504 |

[a] $f_{cov} = [R_{vdW}(S) + R_{vdW}(X) - d(S_{ax}-X)][R_{vdW}(S) + R_{vdW}(X) - R_{cov}(S) - R_{cov}(X)]^{-1}$, where $R_{vdW}$ and $R_{cov}$ are the van der Waals radii and covalent radii of the corresponding atoms (values taken from ref 46); $f_{cov} = 0$ indicates the absence of any covalency, i.e., $d(S_{ax}-X)$ equals the sum of the van der Waals radii; $f_{cov} = 1$ indicates that the $S_{ax}-X$ distance corresponds to the length of a normal S−X single bond. [b] This work. [c] Data from ref 10. [d] Structural data from ref 6; Raman data, this work.

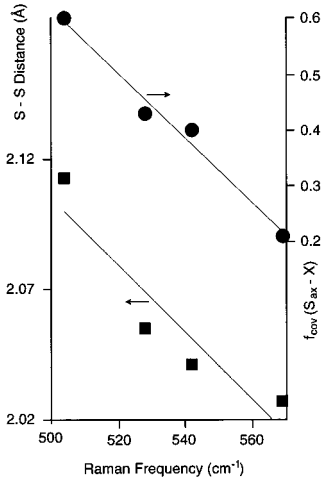


**Figure 3.** The mean $S_{eq}-S_{ax}$ bond lengths (squares) and the covalency ($f_{cov}$) of the $S_{ax}-X$ distance (circles) as functions of the Raman resonance frequency of the $S_{eq}-S_{ax}$ stretch vibration; from left to right: $[Mo_3S_7(dtc)_3]^+$ adducts with $S^{2-}$, $I^-$, $Cl^-$ and $ClO_4^-$ (for definition of $f_{cov}$ see Table 3). The straight lines represent the corresponding linear regression analyses.

**Table 4.** Bond Distances (Å) of the $[Mo_3S_7]^{4+}$ Core Calculated Using DFT at Various Levels of Theory

| | LDA[a] | LDA, Stoll[b] | NL-SCF[c] | expt[d] |
|---|---|---|---|---|
| Mo−Mo | 2.653 | 2.671 | 2.695 | 2.718 |
| Mo−$\mu_3$S | 2.364 | 2.382 | 2.396 | 2.373 |
| Mo−$S_{eq}$ | 2.471 | 2.490 | 2.515 | 2.488 |
| Mo−$S_{ax}$ | 2.424 | 2.443 | 2.460 | 2.415 |
| $S_{eq}-S_{ax}$ | 2.061 | 2.082 | 2.081 | 2.055 |

[a] LDA with VWN approximation. [b] LDA with VWN approximation including Stoll's correction to the correlation. [c] LDA with VWN approximation including gradient-based nonlocal BP corrections to the exchange and correlation potentials. [d] Idealized $C_{3v}$ structural parameters calculated from the X-ray data of **1a**.

and with an $S_{ax}\cdots X$ distance which is significantly shorter than the sum of the corresponding van der Waals radii.

**Theoretical Calculations for Complex Geometry.** The geometries of the $[Mo_3S_7]^{4+}$ core, the complexes $[Mo_3S_{13}]^{2-}$ and $[Mo_3S_7Cl_6]^{2-}$, and the adducts $[Mo_3S_7(L)_3]ClO_4$ and $[Mo_3S_7(L)_3]Cl$ ($L = H-CS_2^-$ representing a simplified model of $dtc^-$) have been optimized using the ADF program at different levels of theory. An idealized $C_{3v}$ symmetry was assumed for all optimized species. The structural parameters calculated for the naked $[Mo_3S_7]^{4+}$ are summarized in Table 4 and are compared with the corresponding experimental values of complex **1a**. As expected, the LDA approximation tends to overestimate the bond strength, leading to an underestimation of the bond distances. The bond lengths generally increase with an improved level of calculation. The Mo−Mo distance is particularly sensitive to the introduction of nonlocal exchange or correlation corrections in these calculations. It is well-known that in the $Mo_3S_7$ complexes the Mo−$S_{eq}$ bonds are generally longer than the corresponding Mo−$S_{ax}$ bonds.[6] This is well reproduced by the calculations. On the basis of simple electrostatic arguments, the coordination of three negatively charged $dtc^-$ ligands to the $[Mo_3S_7]^{4+}$ core should result in an elongation of the Mo−Mo bonds, and consequently, the experimentally determined Mo−Mo lengths in **1a**, **3**, and **4a** are all somewhat longer than the corresponding distances in the hypothetical, isolated $[Mo_3S_7]^{4+}$ fragment. For all other interatomic distances, the values obtained from the LDA calculations and experimental data are in close agreement.

For $[Mo_3S_{13}]^{2-}$,[37] the calculated Mo−Mo and Mo−S distances are again in good agreement with the experimental data (Table 5), although the $S_{eq}-S_{ax}$ distance is significantly overestimated in the calculations. It should be noted that in solid-state structures, the $S_{eq}-S_{ax}$ distances are particularly dependent on further interactions of $S_{ax}$ with additional anionic species. Furthermore, the $S_{eq}-S_{ax}$ bonds are affected by subtle differences of ligand-to-metal $\sigma$ and $\pi$ donations and metal-to-ligand $\pi^*$ back-bonding donations between the various systems (see below) which are apparently not reproduced by DFT calculations performed at the LDA level.

For $[Mo_3S_7Cl_6]^{2-}$,[38] the agreement between theory and experiment is excellent. There is also good agreement between calculated and experimental Mo−Mo and Mo−S bond lengths for the two adducts $[Mo_3S_7(L)_3]Cl$ and $[Mo_3S_7(L)_3]ClO_4$. Again, the calculated $S_{eq}-S_{ax}$ bonds proved to be too long. The calculated value for the intermolecular $S_{ax}\cdots O$ distance (3.20 Å) corresponds approximately to the sum of the van der Waals radii (3.35 Å) and is somewhat longer than the experimental value of 3.01 Å. The $S_{ax}\cdots Cl$ distance in $[Mo_3S_7(L)_3]Cl$ (calculated, 2.69 Å; experimental, 3.00 Å) is significantly underestimated. This overbinding effect is obviously a characteristic of the LDA approximation as reported recently by Ruiz et al. for charge-transfer complexes.[39] Clearly, the introduction of nonlocal corrections to the exchange and correlation functional would significantly improve these results.

**Electronic Structure of $[Mo_3S_7]^{4+}$ and $[Mo_3S_{13}]^{2-}$.** Table 6 lists the orbital energies and the corresponding population analysis for the hypothetical $[Mo_3S(S_2)_3]^{4+}$ fragment. An assignment of the main character of these orbitals is also given. The HOMO, $13e_1$ ($d_{x^2-y^2}$, $d_{xy}$), and the HOMO-2, $11a_1$ ($d_{z^2}$), accommodate the electrons of the three metal−metal single bonds (electron configuration: $a_1^2e^4$). This result is in agreement with earlier calculations on similar compounds.[37,40] The four first unoccupied orbitals consist mainly of d−$\pi^*$ and d−$\sigma^*$ antibonding contributions from the metal atoms. The orbital with highest energy reported in this table ($16e_1$) also contains some antibonding contributions from the $S_2^{2-}$ ligands. The occupied orbitals ranging from $10a_1$ to $12e_1$ all display some degree of electron back-donation from the d orbitals of the Mo

(37) Müller, A.; Wittneben, V.; Krickemeyer, E.; Bögge, H.; Lemke, M. *Z. Anorg. Allg. Chem.* **1991**, *605*, 175.
(38) Klingelhöfer, P.; Müller, U.; Friebel, C.; Pebler, J. *Z. Anorg. Allg. Chem.* **1986**, *543*, 22.
(39) Ruiz, E.; Salahub, D.; Vela, A. *J. Phys. Chem.* **1996**, *100*, 12265.
(40) (a) Müller, A.; Jostes, R.; Cotton, F. A. *Angew. Chem., Int. Ed. Engl.* **1980**, *19*, 875. (b) Müller, A.; Jostes, R.; Jaegermann, W.; Bhattacharyya, R. G. *Inorg. Chim. Acta* **1980**, *41*, 259.

**Table 5.** Bond Distances (Å) for Different Complexes Containing the $[Mo_3S_7]^{4+}$ Core Calculated Using DFT at the LDA Level (VWN Approximation)[a]

| | $[Mo_3S_7(S_2)_3]^{2-}$ [b] | $[Mo_3S_7Cl_6]^{2-}$ [c] | $[Mo_3S_7(L)_3]ClO_4$ [d] | $[Mo_3S_7(L)_3]Cl$ [d,e] |
|---|---|---|---|---|
| Mo−Mo | 2.735 (2.725) | 2.773 (2.758) | 2.687 (2.711) | 2.688 (2.721) |
| Mo-$\mu_3$S | 2.390 (2.367) | 2.370 (2.349) | 2.387 (2.377) | 2.397 (2.368) |
| Mo−$S_{eq}$ | 2.490 (2.486) | 2.496 (2.484) | 2.467 (2.484) | 2.467 (2.481) |
| Mo−$S_{ax}$ | 2.438 (2.420) | 2.403 (2.392) | 2.431 (2.407) | 2.414 (2.409) |
| $S_{eq}$−$S_{ax}$ | 2.067 (2.017) | 2.056 (2.039) | 2.081 (2.027) | 2.120 (2.041) |
| Mo−$Y_{cis}$ | 2.391 (2.405) | 2.429 (2.456) | 2.468 (2.461) | 2.475 (2.471) |
| Mo−$Y_{trans}$ | 2.464 (2.481) | 2.483 (2.501) | 2.507 (2.512) | 2.505 (2.527) |
| $Y_{cis}$−$Y_{trans}$ | 2.105 (2.065) | 3.216 (3.243) | 2.864 (2.870) | |
| $S_{cis}$−C | | | 1.688 (1.711) | 1.687 |
| $S_{trans}$−C | | | 1.680 (1.718) | 1.680 |
| C−H | | | 1.101 | 1.100 |
| $S_{ax}$−X | | | 3.204 (3.013) | 2.693 (3.00) |
| Cl−O | | | 1.516 (1.422)[f] | |
| Cl−O | | | 1.485 (1.427)[g] | |

[a] Corresponding experimental values (from X-ray data) are given in parentheses. [b] Experimental data from ref 37. [c] Experimental data from ref 38. [d] L represents $dtc^-$ (X-ray data) or the corresponding simplified model $H-CS_2^-$ used in the calculations. [e] Experimental data from ref 10. [f] O atom which is in contact with the axial sulfur atoms. [g] Remaining O atoms without any contact to axial sulfur atoms.

**Table 6.** Electronic Structure of $[Mo_3S(S_2)_3]^{4+}$ as Calculated Using DFT at the LDA Level: Occupation of Each Orbital, Symmetry, Ground-State Orbital Energy (*E*, in eV), and Corresponding Charge Distribution[a]

| | | | charge distribn[a] | | | | characteristic groups | |
|---|---|---|---|---|---|---|---|---|
| occup | sym | *E* | Mo | $\mu_3$S | $S_{eq}$ | $S_{ax}$ | $S_2$ bridges | Mo and $\mu_3$S |
| 0 | $16e_1$ | −20.281 | 31 | 5 | 30 | 34 | p−$\pi$*/s*($S_2$) | d−$\pi$*($Mo_3$) |
| 0 | $4a_2$ | −20.594 | 84 | 0 | 1 | 15 | | d−$\sigma$*($Mo_3$) |
| 0 | $15e_1$ | −21.092 | 85 | 1 | 12 | 2 | | d−$\sigma$*($Mo_3$) |
| 0 | $12a_1$ | −21.654 | 43 | 9 | 18 | 30 | p−$\pi$*($S_2$) | $d_{z^2}$ Mo |
| 0 | $14e_1$ | −22.225 | 89 | 4 | 1 | 6 | | d−$\pi$*($Mo_3$) |
| 4 | $13e_1$ | −23.722 | 57 | 11 | 16 | 16 | p−$\pi$*($S_2$) | d−$\sigma$($Mo_3$) |
| 4 | $12e_1$ | −24.209 | 31 | 9 | 54 | 6 | p−$\pi$*($S_2$) | d−$\sigma/\pi$($Mo_3$) |
| 2 | $11a_1$ | −24.357 | 50 | 13 | 9 | 28 | p−$\pi$*($S_2$) | d−$\sigma$($Mo_3$), Mo-$\mu_3$S |
| 2 | $3a_2$ | −24.623 | 43 | 0 | 50 | 7 | p−$\pi$*($S_2$) | d−$\sigma/\pi$($Mo_3$) |
| 4 | $11e_1$ | −25.037 | 49 | 4 | 13 | 34 | p−$\pi$*($S_2$) | d−$\sigma/\pi$($Mo_3$) |
| 2 | $10a_1$ | −25.862 | 54 | 8 | 21 | 17 | p−$\pi$*($S_2$) | d−$\sigma/\pi$($Mo_3$) |
| 4 | $10e_1$ | −26.083 | 26 | 24 | 25 | 25 | p−$\sigma$($S_2$) | Mo-$\mu_3$S |
| 2 | $2a_2$ | −26.548 | 20 | 0 | 27 | 53 | p−$\pi$($S_2$) | d-Mo |
| 4 | $9e_1$ | −26.592 | 21 | 6 | 32 | 41 | p−$\pi$($S_2$) | d-Mo |
| 2 | $9a_1$ | −27.119 | 49 | 47 | 2 | 2 | | Mo-$\mu_3$S |
| 4 | $8e_1$ | −27.513 | 24 | 6 | 23 | 47 | p−$\sigma$($S_2$) | d-Mo |
| 2 | $8a_1$ | −27.604 | 16 | 0 | 54 | 30 | p−$\sigma$($S_2$) | d-Mo |
| 2 | $7a_1$ | −27.911 | 23 | 0 | 30 | 47 | p−$\sigma$($S_2$) | |
| 4 | $7e_1$ | −28.001 | 35 | 8 | 29 | 28 | p−$\pi$($S_2$) | Mo-$\mu_3$S |
| 4 | $6e_1$ | −33.437 | 5 | 0 | 45 | 50 | s−$\sigma$*($S_2$) | |
| 2 | $6a_1$ | −33.677 | 6 | 0 | 43 | 51 | s−$\sigma$*($S_2$) | |
| 2 | $5a_1$ | −35.600 | 11 | 89 | 0 | 0 | | s−$\mu_3$S |
| 4 | $5e_1$ | −37.993 | 3 | 0 | 44 | 53 | s−$\sigma$ ($S_2$) | |
| 2 | $4a_1$ | −38.424 | 6 | 0 | 44 | 50 | s−$\sigma$ ($S_2$) | |
| 2 | $1a_2$ | −57.396 | 100 | 0 | 0 | 0 | | p−$\sigma$*($Mo_3$) |
| 4 | $4e_1$ | −57.403 | 100 | 0 | 0 | 0 | | p−$\sigma$*($Mo_3$) |

[a] The calculation of the charge distribution has been performed using a Mulliken population analysis.

atoms into the empty p−$\pi$* antibonding orbitals of the $S_2^{2-}$ ligands. For the lower energy orbitals, $2a_2$, $9e_1$, $8e_1$, and $8a_1$, some contribution of the metal atoms to the p−$\pi$ and p−$\sigma$ bonding orbitals of the ligands is noted. The interaction of the metal d-orbitals with both antibonding and bonding orbitals of the ligands leads to strong Mo−$S_2$ interactions. At lower energies, the two $\sigma$ bonding orbitals $4a_1$ and $5e_1$, and the two $\sigma$* antibonding orbitals $6a_1$ and $6e_1$, which are mainly located on the $S_2^{2-}$ ligands, exhibit very little metal contribution. It can thus be concluded that the Mo−$S_2$ bonding is almost exclusively due to the interaction of the metal AOs with p−$\pi/\sigma$ and p−$\pi$* orbitals of the $S_2^{2-}$ ligands.

A similar scheme was obtained for the anionic complex $[Mo_3S_{13}]^{2-}$. Here, the three metal−metal single bonds are also described by two occupied orbitals leading to the expected $a_1^2e^4$ configuration.[37] The side-on coordination of the additional (terminal) $S_2$ ligands results in a splitting of the $\pi$* levels to form a strongly MoS bonding $\pi$* orbital in the $MoS_2$ plane and an only weakly interacting $\pi$* orbital perpendicular to this. The HOMOs of the system consist mainly of these latter out-of-plane $\pi$* antibonding contributions from the terminal $S_2^{2-}$ groups. This can be rationalized by adding two electrons to the half-filled $\pi$ antibonding HOMOs of triplet $S_2$ to form the $S_2^{2-}$ ligand. The LUMOs are formed from two p−$\pi$*/$\sigma$* orbitals mainly located on the bridging $S_2^{2-}$ ligands, whereas the subsequent unoccupied orbitals are basically constituted by d−$\pi$* and d−$\sigma$* antibonding contributions of the metal atoms. At lower values of the energy, the electron back-donation from the d orbitals of the Mo atoms into the empty p−$\pi$* in-plane antibonding orbitals of the terminal $S_2^{2-}$ ligands is observed. This back-donation effect, together with the contributions of the metal atoms to the p−$\pi$ and p−$\sigma$ bonding orbitals of the terminal $S_2^{2-}$ ligands (see below), leads to strong Mo−($S_2$) interactions. However, the out-of-plane p−$\pi$* orbitals do not

**Table 7.** Extended Hückel Calculations on LDA-Optimized Geometries of the $[Mo_3S_7]^{4+}$ Core and Corresponding Complexes (Y = S of $S_2^{2-}$, $Cl^-$; L = $H-CS_2^-$): Overlap Population, Frontier Orbital Energy Gap $\Delta E$ (eV), and Net Atomic Charges

| | $[Mo_3S_7]^{4+}$ | $[Mo_3S_{13}]^{2-}$ | $[Mo_3S_7Cl_6]^{2-}$ | $[Mo_3S_7L_3]ClO_4$ | $[Mo_3S_7L_3]Cl$ | $[Mo_3S_7L_3]_2S$[a] |
|---|---|---|---|---|---|---|
| | | | Overlap Population | | | |
| Mo−Mo | +0.1586 | +0.0801 | +0.0823 | +0.1032 | +0.1108 | +0.1057 |
| Mo−$\mu_3$S | +0.5142 | +0.4287 | +0.4377 | +0.4310 | +0.4321 | +0.4342 |
| Mo−$S_{eq}$ | +0.4124 | +0.2899 | +0.2991 | +0.3269 | +0.3256 | +0.3121 |
| Mo−$S_{ax}$ | +0.4318 | +0.3313 | +0.3473 | +0.3547 | +0.3588 | +0.3481 |
| $S_{eq}-S_{ax}$ | +0.6803 | +0.6406 | +0.6585 | +0.6445 | +0.5664 | +0.5470 |
| Mo−$Y_{trans}$ | | +0.3713 | +0.4544 | +0.4100 | +0.4008 | +0.3915 |
| Mo−$Y_{cis}$ | | +0.4214 | +0.4945 | +0.4246 | +0.4178 | +0.4145 |
| $Y_{trans}-Y_{cis}$ | | +0.5788 | −0.0096 | −0.1131 | −0.1151 | −0.1104 |
| $S_{ax}$−O | | | | −0.0003 | | |
| $S_{ax}$−Cl | | | | | +0.0290 | |
| $S_{ax}-S^{2-}$ | | | | | | +0.0471 |
| $\Delta E_{homo-lumo}$ | 0.996 | 0.623 | 0.938 | 0.056 [b] | 0.511 | 0.237 |
| | | | Net Atomic Charge | | | |
| $\mu_3$S | +0.289 | −0.189 | −0.122 | −0.038 | −0.078 | −0.119 |
| Mo | +0.562 | +0.087 | +0.125 | +0.237 | +0.213 | +0.171 |
| $S_{eq}$ | +0.325 | −0.106 | −0.050 | +0.031 | −0.025 | −0.076 |
| $S_{ax}$ | +0.351 | −0.074 | −0.003 | +0.057 | +0.031 | −0.008 |
| $Y_{trans}$ | | −0.264 | −0.359 | −0.028 | −0.047 | −0.102 |
| $Y_{cis}$ | | −0.246 | −0.339 | −0.016 | −0.042 | −0.099 |
| C | | | | +0.020 | +0.008 | |
| H | | | | +0.017 | +0.013 | |
| Cl | | | | +0.740 | **−0.373** | |
| O(1)[c] | | | | **−0.418** | | |
| O(2)[d] | | | | −0.405 | | |
| $S^{2-}$ | | | | | | **−0.250** |

[a] The structural parameters of the X-ray study reported in ref 6 were used. [b] This small value for the frontier orbital gap is a consequence of the long distance between the cation and the anion (3.204 Å). [c] O atom which is in contact with the axial sulfur atoms. [d] Remaining O atoms without any contact to axial sulfur atoms.

contribute much to the metal−ligand bond. For the bridging $S_2^{2-}$ ligands, the back-donation effect from the d orbitals of the metal into the $\pi^*$ antibonding orbitals of these ligands is described by more stable orbitals than in the case of the terminal $S_2$ groups. These orbitals also have the above-mentioned interaction between the metal orbitals and the p−$\pi/\sigma$ bonding orbitals of the terminal $S_2^{2-}$ ligands, whereas the same type of interaction for the bridging $S_2$ ligands appears at more negative energies.

These results indicate a considerable competition between the bridging and terminal $S_2$ ligands as back-donation acceptors. According to the crystal structure, the S−S bond in the $S_2$ bridges is shorter than in the terminal $S_2$ ligands, so a higher population of the $\pi^*$ level must be assumed for the latter. The calculated electronic structure and the atomic charges (which are more negative on the terminal $S_2$ groups) now allow the experimental observations to be rationalized.

**Extended Hückel Calculations on LDA-Optimized Geometries.** Standard extended Hückel calculations[27] have been performed for all the LDA-optimized geometries. The results are summarized in Table 7. The main features deduced from these calculations are the following. The overlap population between Mo and $S_{ax}$ is larger than that between Mo and $S_{eq}$. This observation is in agreement with the corresponding difference in the Mo−S bond lengths (Table 2) and can be considered to account for the increased lability of the equatorial sulfur atoms.[5,36,41] In addition, the overlap population between Mo and $Y_{cis}$ is larger than that between Mo and $Y_{trans}$ (Y = S of a terminal $S_2^{2-}$, $Cl^-$). Compared to the equatorial S atoms, the net atomic charges of the axial S atoms are more positive. Related differences are observed for the ligating atoms Y in the cis and trans positions, where a less negative net atomic charge is found for the cis position.

The results for the $[Mo_3S_7L_3]^+$ adducts with $ClO_4^-$ and $Cl^-$ and for the dimer $[Mo_3S_7L_3]_2S$ (L = $H-CS_2^-$ representing a simplified model of $dtc^-$) show increasing overlap populations and decreasing charge differences for the axial sulfur atoms and the nucleophile in the order $ClO_4^-$, $Cl^-$, $S^{2-}$.

The reactivity of the $[Mo_3S_7]^{4+}$ fragment toward general nucleophilic reagents has been investigated by means of a modeling study using the EHPROP formalism.[28,29] Figure 4 presents the results of a simulated nucleophilic attack on the $[Mo_3S_7]^{4+}$ core. The most reactive sites are described by isoenergy surfaces, which are built from all the points exhibiting the same value of the intermolecular interaction energy $E_{int}$ in the vicinity of the cluster. This interaction energy may be taken as a local reactivity index. The deepest minimum (−440 kcal/mol) corresponds to the anionic binding site located between the three axial sulfur atoms. Additional minima of −422 and −419 kcal/mol correspond to the cis und trans positions of the ligating atoms of a peripheral ligand. It is noteworthy that, for a single nucleophile, the midpoint between these cis and trans positions (having an energy of −418.5 kcal/mol) corresponds to a saddle point rather than to a minimum.

**Lability of $S_{eq}$ vs $S_{ax}$ in $[Mo_3S(S_{eq}-S_{ax})_3]^{4+}$.** In a previously reported mass spectrometric study, evidence was provided for a different lability between the axial and the equatorial sulfur atoms in $[Mo_3S(S_{eq}-S_{ax})_3]^{4+}$ complexes.[41] In the present investigation a theoretical approach based on a three-step procedure was used to correlate these findings with the electronic properties of the complex core.

First, the energy of a $[Mo_3$-$\mu_3$S-$(S_{eq}-S_{ax})_2$-$S_{ax}]^{4+}$ moiety (Figure 5a, structure **I**) having a vacant $S_{eq}$ site was calculated in DFT using the fixed structural parameters of the LDA-optimized $[Mo_3S_7]^{4+}$ geometry. The same procedure was carried out for an analogous $[Mo_3$-$\mu_3$S-$(S_{eq}-S_{ax})_2$-$S_{eq}]^{4+}$ moiety (structure **II**) having a vacant $S_{ax}$ site. The energies of **I** and **II** were calculated at two different levels of theory, LDA and NL-

(41) Hegetschweiler, K.; Caravatti, P.; Fedin, V. P.; Sokolov, M. N. *Helv. Chim. Acta* **1992**, *75*, 1659.

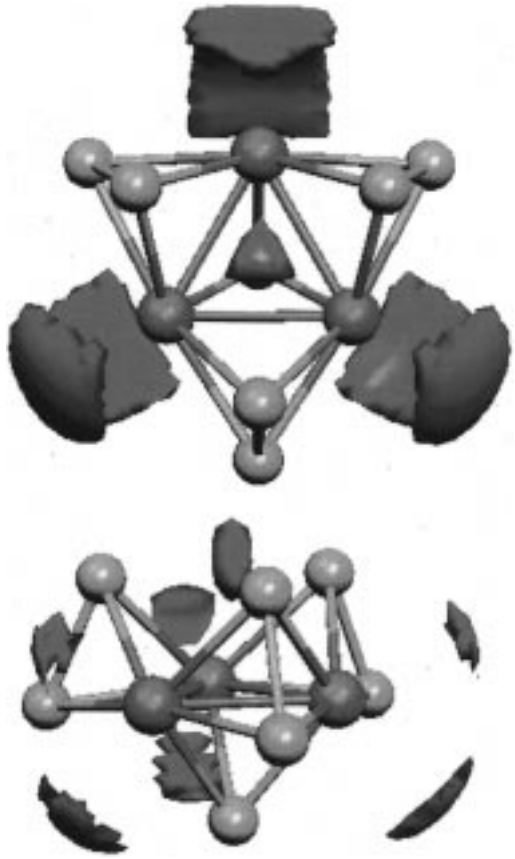

**Figure 4.** Two different views of the $[Mo_3S_7]^{4+}$ core from the top (a, above) and from the side (b, below) with EHPROP isoenergy surfaces for a nucleophilic attack at −400 kcal/mol and −415 kcal/mol, respectively.

SCF (BP). It should be noted that these geometries were not reoptimized, and that the evaluated energies do not represent the corresponding minima. Both levels of theory revealed a significantly lower energy for structure **I**. The energies for the recombination of the two fragments **I** and **II** with a neutral sulfur atom (Figure 5a) yielding the entire $[Mo_3S_7]^{4+}$ cluster core were then calculated, once again revealing a significantly higher bond energy for **I**. Obviously, an equatorial vacant site seems to be preferred over an axial one, and consequently equatorial S atoms appear to be more labile than axial ones.

Second, a DFT linear transit calculation with constrained geometries was carried out between structures **I** and **II** (Figure 5b) at the LDA level. These calculations consisted of an inspection of the potential surface taking the transfer of an S atom from the equatorial to the axial position as the reaction coordinate. The changes in energy of this system along the reaction path together with the corresponding structures are shown in Figure 5b. For the most stable structure, the geometry was then relaxed and reoptimized (Figure 5c). In this relaxed structure, the optimal position for the S atom is located out of the plane defined by the three Mo atoms, that is, this system prefers to have a single $\mu_2$-S bridge in an axial rather than an equatorial position.

Finally, the geometries of both structures **I** and **II** were optimized at the LDA level of theory. The same final geometry was obtained, having a vacant site in the equatorial position, confirming though the existence of only one absolute minimum in the reaction path.

**Lability of $Cl_{trans}$ and $Cl_{cis}$ in $[Mo_3S_7Cl_6]^{2-}$.** It has been shown previously[3,4,7] that an attack of a nucleophilic agent on a complex containing the $[Mo_3S(S_2)_3]^{4+}$ core can also result in the substitution of the peripheral ligands. In order to shed light on the possible mechanism of such substitution reactions, we applied a three-step procedure (similar to the one described above) to the model complex $[Mo_3S(S_2)_3Cl_6]^{2-}$. Due to the high coordination number of Mo in this complex, a dissociative substitution mechanism was proposed with $[Mo_3S_7Cl_5]^-$ as a hypothetical intermediate. The structural parameters of two such fragments **III** and **IV** (Figure 6a), having the single chloro ligand in either the trans or the cis position, were deduced from the LDA-optimized geometry of $[Mo_3S(S_2)_3Cl_6]^{2-}$. The corresponding energies of **III** and **IV** were evaluated, and bond energies were calculated for the recombination with a $Cl^-$ ligand (Figure 6a). A scan of the potential energy surface for a set of intermediates between **III** and **IV** was then performed (Figure 6b), and finally, the geometries of the two located minima (A and E) were reoptimized (Figure 6c).

Our results show that structure **III** is more stable than structure **IV** by 4.8 kcal/mol, indicating that there is only a slight preference for a vacant site in the trans rather than the cis position. Also, the gain in energy resulting from the addition of a Cl atom to the cis position is slightly higher. The energies, calculated for the transition from **III** to **IV**, together with the corresponding structures are shown in Figure 6b. Two local minima could be assigned (A and E): the first minimum (structure A) has a vacant cis position while the second minimum (E) has a vacant trans position. Since all these energies correspond to structures with constrained geometries, additional geometry optimizations were performed for the two minima (A and E) and the transition state C lying in between. After relaxation of the structural parameters, E converged toward an energy minimum with the vacant site still in the trans position. However, the structures A and C now converged toward the same minimum.

It is interesting to compare the results of the DFT calculations and the semiempirical EHPROP procedure reported above. According to the EHPROP calculations a nucleophilic attack on the cis position of the $[Mo_3S_7]^{4+}$ moiety seems to be favored. The minimum of the interaction energy $E_{int}$ lies at −422.0 kcal/mol for the cis and at −419.0 kcal/mol for the trans position. This result is in agreement with the ADF calculations reported above showing that in $[Mo_3S_7Cl_6]^{2-}$ $Cl_{trans}$ is slightly more labile than $Cl_{cis}$.

## Discussion

**Structure−Energy Correlations.** The X-ray results presented in this paper together with the data from previous investigations reveal two characteristic structural properties of the $[Mo_3S_7(dtc)_3]^+$ entity: (i) In the bridging disulfido groups, the Mo−S bonds of the axial (out-of-plane) sulfur atoms are significantly shorter than the Mo−S bonds of the equatorial (in-plane) sulfur atoms. (ii) In the chelating $dtc^-$ ligand, the Mo−S bonds of the ligating sulfur atoms in the cis position (with respect to $\mu_3$-S) are slightly shorter than the Mo−S bonds of the corresponding atoms in the trans position. Analogous behavior was also observed for $[Mo_3S_7]^{4+}$ complexes with other peripheral ligands, such as $S_2^{2-}$, $Cl^-$, and $Br^-$.

With regard to the extended theoretical calculations presented in this work, it must of course be emphasized that, for the sake of simplicity, heavy-atom ligands such as $Br^-$ or $I^-$ or multiatom ligands such as $dtc^-$ were not considered and were replaced by simpler models such as $Cl^-$, $S_2^{2-}$, or L (=H−$CS_2^-$). However, because of the structural conformity of all $[Mo_3S_7]^{4+}$ derivatives, it is rather likely that these results are generally valid, thus

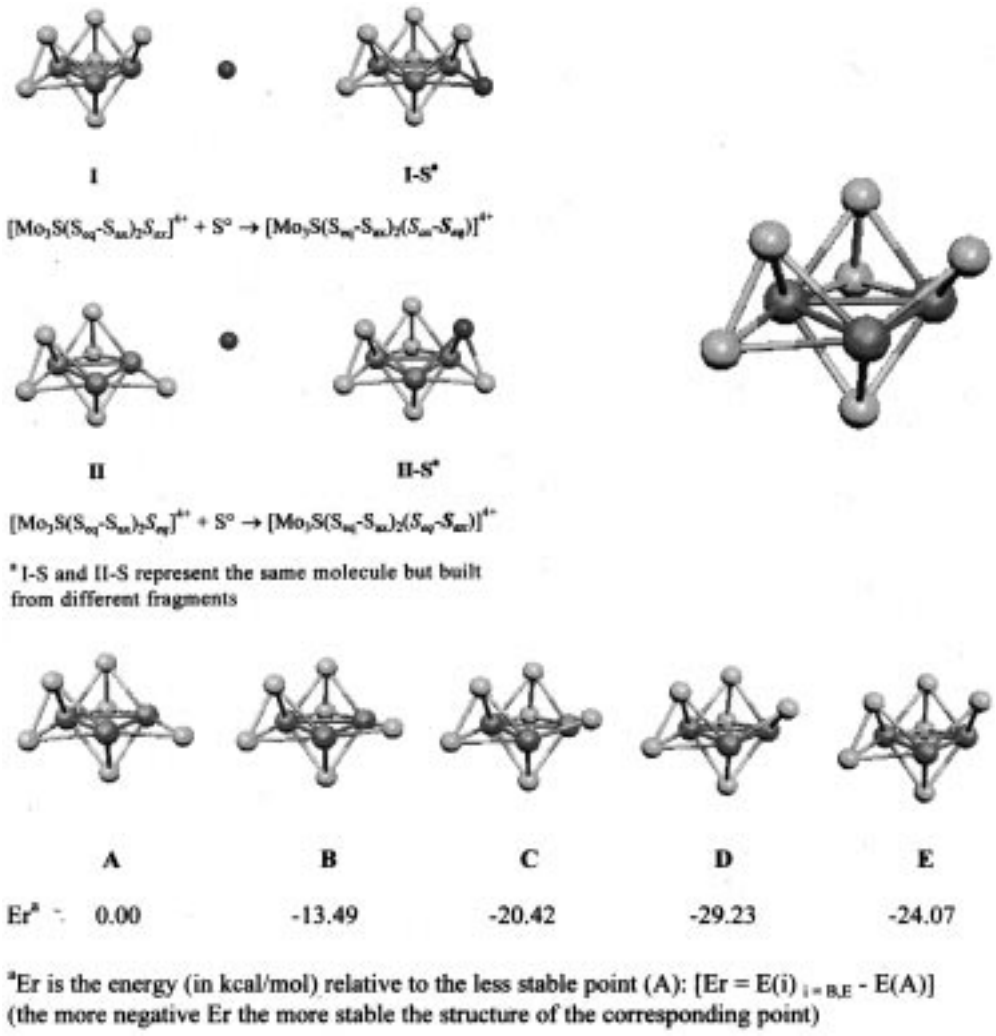


**Figure 5.** Different labilities of $S_{eq}$ and $S_{ax}$ in terms of bond energies. (a, above left) Structures of the $[Mo_3\text{-}\mu_3S\text{-}(S_{eq}-S_{ax})_2\text{-}S]^{4+}$ moiety (fragments **I** and **II**), having either a vacant $S_{eq}$ or a vacant $S_{ax}$ site. (b, below) Various steps during the DFT linear transit calculation: from $[Mo_3S(S_{eq}-S_{ax})_2\text{-}S_{eq}]^{4+}$ to $[Mo_3S(S_{eq}-S_{ax})_2\text{-}S_{ax}]^{4+}$. (c, above right) DFT (LDA) optimized geometry of structure D.

providing a solid basis for the understanding of the observed reactivity. The calculations clearly established that the shorter $Mo-S_{ax}$ bonds (compared to $Mo-S_{eq}$) go together with higher bond energies, and they can be explained on the basis of electronic properties. One would thus expect that a sulfur atom in the equatorial position is more labile and will be eliminated preferentially. Moreover, it is of particular interest that, after dissociation, the remaining $\mu_2$-S atom retains the axial position rather than moving to an intermediate location. Consequently, an entering nucleophile will fill the vacant equatorial position, thus giving rise to a selective substitution process. In a recent publication, some of us have indeed demonstrated that it is possible to substitute selectively the three equatorial sulfur atoms of $[Mo_3S_7(dtc)_3]^+$ by three selenium atoms.[42] The exclusive substitution of the equatorial positions has been confirmed by an X-ray analysis. Moreover, collision-induced decomposition experiments in an ion cyclotron resonance experiment resulted in selective elimination of $Se_2$ from this complex, confirming thus the expected higher lability of atoms in equatorial positions.[41]

For the substitution of peripheral ligands, our calculations are less conclusive. The results from the structural analysis show that ligating atoms in the cis position form shorter bonds to the Mo atoms than those in the trans position. This is consistent with the higher bond energy calculated for $Mo-Cl_{trans}$ in $[Mo_3S_7Cl_6]^{2-}$. A recent study where the reaction of $[Mo_3S_7(H_2O)_6]^{4+}$ with a 10-fold excess of $Cl^-$ was investigated did indeed reveal the expected biphasic kinetics for the ligand substitution.[43] However, it must be emphasized that the calculated difference in the Mo−Cl bond energies is rather small (<5 kcal/mol). In contrast to substitution of an equatorial sulfur atom, discussed above, it is rather likely that, in a preparative procedure, the substitution of a peripheral $Cl^-$ ligand is under thermodynamic rather than kinetic control, and that the structure of the product is governed by the electronic and steric properties of the entering nucleophile. As is well-known, $[Mo_3S(S_2)_3Br_6]^{2-}$ reacts with a variety of monodentate and bidentate ligands with complete retention of the $[Mo_3S(S_2)_3]^{4+}$ core and this substitution is stereoselective.[4,7] However, in the reaction with the monodentate aniline, the substitution of only three $Br^-$ ions in

(42) (a) Fedin, V. P.; Mironov, Yu. V.; Sokolov, M. N.; Virovets, A. V.; Podberezskaya, N. V.; Fedorov, V. Ye. *Zh. Neorg. Khim.* **1992**, *37*, 2205. (b) Fedin, V. P.; Sokolov, M. N.; Virovets, A. V.; Podberezskaya, N. V.; Fedorov, V. Ye. *Polyhedron* **1992**, *11*, 2395.

(43) Fedin, V. P.; Lamprecht, G. J.; Sykes, A. G. *J. Chem. Soc., Chem. Commun.* **1994**, 2685.

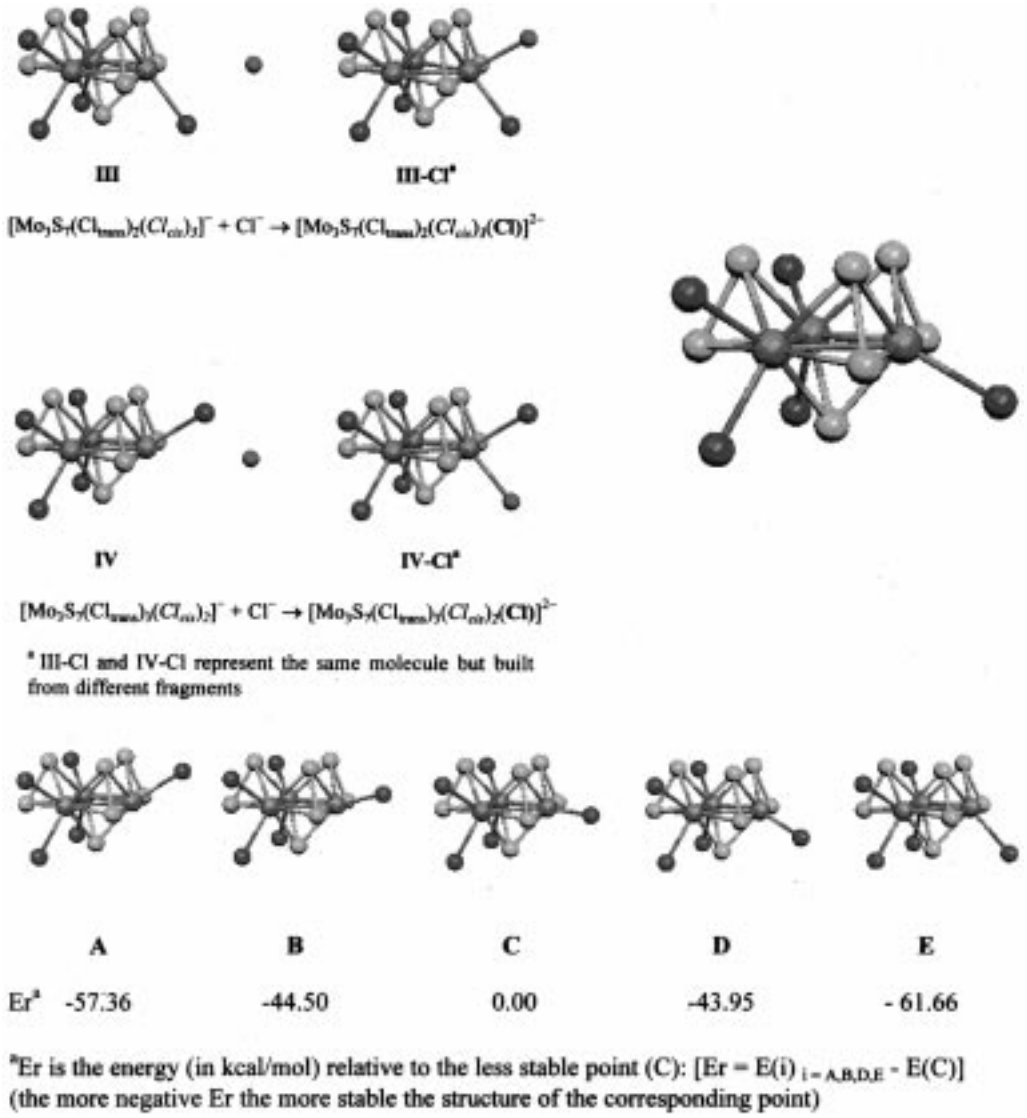


**Figure 6.** Different labilities of $Cl_{trans}$ and $Cl_{cis}$ in terms of bond energies. (a, above left) Structures of the [$Mo_3$-$\mu_3$S-($\mu S_2$)$_3$-*Cl*]$^-$ moiety (fragments **I** and **II**), having either a vacant $Cl_{cis}$ or a vacant $Cl_{trans}$ site. (b, below) Various steps during the DFT linear transit calculation: from $[Mo_3S_7(Cl_{trans})_3(Cl_{cis})_2]^-$ to $[Mo_3S_7(Cl_{trans})_2(Cl_{cis})_3]^-$. (c, above right) DFT (LDA)-optimized geometry of structure E.

the less labile cis positions has been observed.[44] According to the results of our calculations, this selectivity should therefore be interpreted in terms of the formation of the thermodynamically most stable isomer.

**The Binding of Anions to the Three Axial Sulfur Atoms.** In the past few years, several reports have appeared in the literature on the preparation and structural characterization of compounds containing the $[Mo_3S_7(dtc)_3]^+$ cluster complex together with different counterions.[3,6,10,31−33] In the present paper, we have extended this work to include the derivatives with $ClO_4^-$ (**4**), $NO_3^-$ (**5**), and $SO_4^{2-}$ (**6**). In addition we have reinvestigated compound **1**, having $I^-$ as counterion in order to deduce more precise structural parameters. We also report a more convenient protocol for the preparation of the dimeric species $[Mo_3S_7(dtc)_3]_2S$ (**3**). X-ray structural data are now available for **1a**, **2**, **3**, **4a**, and **6**[35] and for the adducts with $Cl^-$ and $TCNQ^-$.[10,31] In all these structures a direct interaction is observed between the anion and the three axial sulfur atoms of the cluster cation. It is of particular interest to compare the structures with counterions of similar size and geometry but carrying different charges. The structure of $[Mo_3S_7(dtc)_3]Cl$ comprises a 1:1 adduct, whereas $[Mo_3S_7(dtc)_3]_2S$ (**3**) exists as a dimeric aggregate. Likewise in **4a**, the mononegative $ClO_4^-$ ion is bound to one single cluster entity whereas the doubly charged $SO_4^{2-}$ binds to a total of four cluster entities (Figure 2). These observations seem to indicate that the increased negative charge gives rise to an increased coordination number of the counterion. Considering the wide structural diversity of potential anions, such correlations could prove helpful for the design of novel solid-state structures. However, the reported crystal structure of $(C_{18}H_{30}N_3)_2[Mo_3S_7(Hmsa)_3]$-$[Mo_3S_7(Hmsa)_2(msa)]Br\cdot 6H_2O$ ($H_3msa$ = 2-mercaptosuccinic acid)[4] shows that a straightforward strategy for the synthesis of such aggregates may be difficult. Due to the presence of noncoordinating carboxylates, we expected the $[Mo_3S_7(Hmsa)_2(msa)]^{3-}$ entity to serve as a promising building block for a self-assembling structure. However, the X-ray analysis revealed no interaction between the peripheral carboxylates and the anionic binding site of the cluster anion at all. Instead, the incorporation of an additional $Br^-$ ion undergoing binding interactions to two cluster entities was observed (Figure 7).

(44) Fedin, V. P.; Mironov, Yu. V.; Virovets, A. V.; Podberezskaya, N. V.; Fedorov, V. Ye. *Polyhedron* **1992**, *11*, 2083.

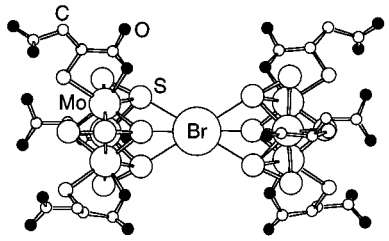


**Figure 7.** Ball and stick representation of the crystal structure of the dimeric $\{[Mo_3S_7(Hmsa)_3]Br[Mo_3S_7(Hmsa)_2(msa)]\}^{6-}$ ($H_3msa$ = 2-mercaptosuccinic acid) according to the X-ray data given in ref 4. Br, Mo, and S atoms are shown as spheres with decreasing diameter in this order. C and O atoms are shown as small open and closed spheres, respectively.

With regard to the still unknown selectivity and stability of such interactions, it would be of interest to have a better understanding of the nature of the anion$-S_{ax}$ bonding. The calculations presented in this investigation (Table 7) indicate that, in the $ClO_4^-$ adduct **4**, this bonding is almost entirely ionic. A positive charge is located on the axial sulfur atoms of $[Mo_3S_7(dtc)_3]^+$, and the binding to the anion can be described simply in terms of an electrostatic attraction. However, for the dimeric $S^{2-}$ derivative **3**, the calculations indicate a significant release of electron density from the anion to the cation. This is manifested by significantly reduced net atomic charges and substantially enlarged overlap populations for the anion$-S_{ax}$ bonds (Table 7). This interpretation is nicely confirmed by the experimental results presented in this paper. The frequency of the $S_{ax}-S_{eq}$ stretching vibration underwent a monotonic decrease $ClO_4^- > Cl^- > I^- > S^{2-}$, indicating significant reduction of the force constants in this direction. This finding is correlated with some increase in the $S_{ax}-S_{eq}$ bond distance and a significant decrease of the $S_{ax}\cdots X$ distance when compared with the sum of the corresponding van der Waals radii (Table 3 and Figure 3). According to Pearson's concept of hard and soft acids and bases,[45] the above-noted order also corresponds to a decrease in the hardness of the anion. The results of our present investigation allow us to draw the general conclusion that these interactions are predominantly ionic for hard counterions such as $NO_3^-$ and $ClO_4^-$, whereas significant covalency is observed for soft nucleophiles such as $I^-$ and $S^{2-}$.

**Acknowledgment.** Generous financial support by the Swiss National Science Foundation (Projects 20-49037.96, 21-30773.91, and 7GUPJ038508) is gratefully acknowledged. We are indebted to Dr. Peter Osvath (CSIRO, Melbourne) for his careful reading of the manuscript.

**Supporting Information Available:** Listings of crystallographic data, atomic coordinates, anisotropic displacement parameters, positional parameters of hydrogen atoms, bond distances and bond angles, and bond energies and calculated structural parameters of the DFT (LDA) optimized geometries $[Mo_3S(S_{eq}-S_{ax})_2\text{-}S]^{4+}$ and $[Mo_3S_7Cl_5]^-$ (18 pages). Ordering information is given on any current masthead page.

IC971214T

(45) Pearson, R. G. *J. Am. Chem. Soc.* **1963**, *85*, 3533.
(46) Batsanov, S. S. *Russ. J. Inorg. Chem.* **1991**, *36*, 1694.